In situ and operando TEM study of Pt-based hollow nanocatalysts: tracking morphological changes and reaction products during CO2 hydrogenation

Josephine Rezkallah, Simona Moldovan, Xavier Sauvage

In situ and operando TEM study of Pt-based hollow nanocatalysts: tracking morphological changes and reaction products during CO_2 hydrogenation

Josephine Rezkallah [a,b,*], Simona Moldovan [a], Xavier Sauvage [a]

[a] Groupe de Physique des Matériaux (GPM), Univ Rouen Normandie, INSA Rouen Normandie, CNRS UMR 6634, 76000 Rouen, France ; xavier.sauvage@univ-rouen.fr, simona.moldovan@univ-rouen.fr

[b] Laboratoire de Réactivité et de Chimie des Solides (LRCS), Univ Picardie Jules Verne, CNRS UMR 7314, 80000 Amiens, France

*corresponding author: josephine.rezkallah@u-picardie.fr

Abstract

The catalytic hydrogenation of CO_2 using cost-effective renewable H_2 presents a promising pathway for sustainable methanol synthesis. Due to their remarkable stability and resistance, Pt-based catalysts have gained attention despite the challenges related to their high cost and deactivation mechanisms. In this paper, we investigate the overall thermal stability and deactivation mechanisms of Pt-based hollow nanospheres (HNS) during the CO_2 hydrogenation reaction using the in situ and operando Transmission Electron Microscopy (TEM) approach. The morphological characterization via STEM-HAADF and electron tomography (ET) confirms the presence of porous HNS with open channels which ensure the efficient gas diffusion. The simultaneous analysis of the reaction products using residual gas analyzer (RGA) reveals the production of both formic acid (HCO_2H) and methanol (CH_3OH), which indicate the dominance of the Formate pathway. The morphological evolution studies show prove the sintering of nanoparticles (NPs) forming the catalysts shell via particle and atomic migration along with the collapse of HNS at elevated temperatures. This study provides critical insights into the deactivation mechanisms of Pt-based HNS, contributing to the design of more stable and efficient catalysts for CO_2 hydrogenation to methanol.

Key words: CO_2 hydrogenation, hollow nanospheres, catalysts, in situ and operando TEM, deactivation mechanisms

1. Introduction

With the progress in capture technologies, the utilization of CO_2 through cost-effective renewable H_2 in catalytic hydrogenation emerges as a promising approach to reduce the carbon footprint of industrial processes. In this context, hydrogenation present a promising pathway to produce various industrially interesting compounds. These compounds include methane [1], a crucial renewable energy source, carbon monoxide [2], commonly used in large-scale chemical production, oxygenates such like methanol [3], ethanol [4] and Formate [5], as well as long-chain hydrocarbons [6] which can be obtained through direct routes [7].

The hydrogenation of CO_2 into alcohol gains the interest of both chemical industry and scientific community.

Among the various alcohols, methanol, as a prominent C_1 alcohol, holds particular importance as it can serve as a precursor to produce a wide range of chemical compounds through further processing. The hydrogenation of CO_2 to methanol is an exothermic reaction that occurs more favorably under mild temperatures and high pressures. To activate CO_2, which has an inert nature, temperatures above 150 °C are necessary for methanol synthesis. The process of methanol synthesis can proceed through two pathways: 1) the Formate pathway and 2) the reverse Water-Gas Shift reaction (rWGS) + CO hydrogenation pathway [8]. The first pathway centers around the formation of a formate (*HCOO) intermediate during CO_2 hydrogenation. This formate intermediate eventually leads to the production of CH_3OH through the breaking of the C-O bond, with involvement of $*H_2CO$ or $*HCO_2H$ intermediates. This pathway is termed the *Formate pathway*. The second pathway involves the production of a CO intermediate through the reverse-water-gas-shift (RWGS) reaction ($CO_2 + H_2 \rightarrow CO + H_2O$). This intermediate is then hydrogenated to produce CH_3OH, and we refer to this as the *CO-Hydro pathway*. In either pathway, the activated CO_2 molecule reacts with adsorbed atomic H, and this interaction determines the direction the reaction takes [9]. The Formate pathway is considered more favorable since the rWGS + CO hydrogenation pathway can result in a higher selectivity for CO due to the rWGS reaction [10]. The proper selection of a catalyst is essential for controlling the reactivity of CO_2 and H_2, as well as determining the specific reaction pathway to achieve desired outcomes.

Recent advancements in Pt-based catalyst research have been dedicated to exploring the optimal conditions for the CO_2 hydrogenation reaction to produce methanol. Toyao et al [11]. conducted a study on a Pt (3)/MoO_x (30)/TiO_2 catalyst, consisting of 3 wt. % of Pt supported on MoO_x/TiO_2. The interaction between Pt and MoO_x was proved to facilitate the reaction at a low temperature of 150 °C and a pressure of 60 bar in a batch reactor, resulting in an impressive methanol yield of 73% and a methanol selectivity of around 91%. In another contribution by Men et al. [12], a Pt/film hybrid catalyst featuring highly dispersed Pt NPs over In_2O_3 was investigated for CO_2 hydrogenation using a dielectric barrier discharge (DBD) plasma reactor. Remarkable results were achieved, including a 37% conversion of CO_2 and a methanol selectivity of 62.6% at 1 atm and 30 °C. The exceptional dispersion of Pt NPs played a leading role in promoting enhanced methanol activity, while the high-energy electrons generated by the DBD plasma facilitated the reaction to occur under mild conditions (relatively low temperature ~ 150°C). Furthermore, Gutterød et al. [13] studied the methanol formation mechanism at 170°C under atmospheric pressure over Pt NPs dispersed over Zr-based metal-organic framework (MOF). Even though the methanol yield was not high, this study is considered one of the few that demonstrated significant methanol formation from CO_2 hydrogenation over a Pt-based catalyst, especially when the support alone was inactive.

These studies open new possibilities for the use of Pt-based catalysts in methanol synthesis. The high cost of Pt and its limited availability are main challenges for its applications. To resolve this issue, experimental and theoretical studies have been done to improve its catalytic performance [14]. One of the most effective strategies for improving Pt's catalytic efficiency is increasing its surface area, since larger surface areas provide more active sites for catalytic reactions. Novel structural designs such as hollow, porous, and dendritic

structures [15], [16], [17] have been shown to significantly enhance the specific surface area, thereby improving catalytic activity.

However, catalyst deactivation is a major challenge in heterogeneous catalysis, which leads to a degradation in performance over time. The deactivation can occur via through multiple mechanisms, mainly categorized into six different types: (1) poisoning, (2) fouling, (3) thermal degradation, (4) formation and transport of volatile compounds or leaching, (5) vapor-solid and/or solid-solid reactions, and (6) crushing. For HNS catalysts, thermal degradation is particularly critical specially since the shell in formed by interconnected NPs. At high temperatures, NPs tend to coalesce leading to densification, collapse of the hollow morphology and therefore, a reduction in the surface area [18], ultimately compromising catalytic performance. Understanding these deactivation mechanisms is highly necessary for the development of catalytic systems with optimized stability and efficiency. By identifying the key factors causing catalyst degradation, researchers are able to design materials with improved resistance to deactivation and a sustained catalytic activity. Pt-based nanomaterials are used in a wide range of catalytic applications, including selective hydrogenation reactions and proton-exchange membrane fuel cells (PEMFCs), all operating in a H_2 rich environments. In order to investigate the catalyst's behavior in a reducing environment, CO_2 hydrogenation was selected as a model reaction. This choice is not only motivated by the reaction's relevance as a representative hydrogenation process but also by its importance in sustainable energy applications.

In this paper, we study the thermal stability and potential poisoning effects of Pt-based HNS during CO_2 hydrogenation reaction. For these investigations, we use the in situ and operando TEM approach. This latter allows real-time monitoring of the catalyst's evolution under near-reaction conditions while simultaneously providing a qualitative analysis of the reaction's products. With this methodology, we offer valuable insights into the morphological transformation of the HNS in response to temperature variations, a critical factor influencing their stability and performance. Although the in situ and operando TEM technique enables the direct observation of catalyst evolution in a realistic environment, it presents also certain limitations. Among these limitations is its inability to precisely quantify the absolute concentration of specific gas species. Therefore, this approach can not be used for quantitative measurements such as determining reaction yield. However, its capability to bridge the gap between ex situ studies and real catalytic processes makes it a powerful tool for understanding structure-performance relationships in heterogeneous catalysis. The originality of this work lies in both the innovative experimental approach, which integrates in situ and operando Transmission Electron Microscopy (TEM) with catalytic analysis, and the unique Pt-based HNS system investigated, providing novel insights into the behavior of hollow nanocatalysts under reaction working conditions.

2. Materials and methods

The synthesis of Pt-based hollow nanospheres (HNS) follows the galvanic replacement method using Co nanoparticles as sacrificial templates. Cobalt (Co) NPs are first synthesized and dispersed into solution. Then, a Pt precursor (H_2PtCl_6) is introduced, leading to selective

oxidation and dissolution of Co while Pt is simultaneously deposited, forming hollow nanospheres. The final Pt-based HNS are collected, washed and characterized.

Imaging and analysis were carried out using a double Cs-corrected JEOL® ARM200CF transmission electron microscope (TEM). High-angle annular dark-field scanning TEM (HAADF-STEM) imaging was used with a camera length of 8 cm. Images (1024 x 1024 px) were acquired with an exposure time of 20 µs per pixel. Elemental analysis was carried out using STEM-EDS with spectra acquired at a dwell time of 0.02 ms. The 3D morphology of the particles was analyzed using electron tomography (ET) in STEM-HAADF mode with tilt series acquired from -67° to +68° at 3° increments. Image stacks were acquired and aligned using 5 nm Au NPs as fiducial markers. The tomographic reconstruction was performed using TomoJ (an ImageJ plugin) and the OS-SART (ordered subset simultaneous algebraic reconstruction technique) algorithm. Details on the synthesis procedure and ET analysis are thoroughly described in a previous study [18].

A closed Environmental Cell (E-cell) system ("Atmosphere" from Protochips®) was used for in situ TEM to monitor the real-time morphological evolution of the catalyst during CO_2 hydrogenation under controlled temperature, gas composition, and pressure. A thermal treatment was applied to the Pt-based HNS under a CO_2/H_2 gas mixture at a 4:1 ratio, a pressure of 1 bar and with a heating rate of 0.4°C/s. STEM-HAADF micrographs were acquired at temperature increments of 20-50°C using the same parameters as the initial analysis except for an exposure time of 12 µs/pixel.

The morphological evolution of Pt-based HNS was also investigated under isothermal conditions at 180°C while maintaining the same CO_2 hydrogenation reaction parameters. The system was heated to 180°C at 1°C/s rate. Then this temperature was maintained for a 3-hour thermal treatment where STEM-HAADF images were collected every 20 minutes. In order to analyze simultaneously the reaction products, an RGA was positioned on the E-cell's exit. This system allows gas phase analysis at trace level (ppm) and consists of a mass spectrometer and differential pumping system. It operates at low pressures ($\sim 10^{-6}$ mbar) to minimize ion collisions with a mechanical and a turbomolecular pump to regulate the gas pressure at the exit of the E-cell.

The RGA operates in two modes: "Analog scan" for the products identification and "Time vs. Pressure" for the monitoring of the products evolution over time. An analog scan refers to a continuous measurement mode in which the instrument systematically scans across a predefined range of mass-to-charge (m/z) ratios. During this scan, the RGA records the partial pressure (PP) associated to each m/z value. By capturing a full spectrum of the evolving gas phase species during this reaction, this approach enables the identification of key reaction products and intermediates. It offers critical insights into the underlying reaction pathway of CO_2 hydrogenation. The presence of specific products (e.g., water H_2O, formic acid HCO_2H and methanol CH_3OH) directly reflect the dominate Formate reaction pathway under the given experimental conditions. To identify the reaction onset temperature for each product and try to correlate the morphological evolution of the catalysts to the reaction response, the RGA is operated in "Pressure vs time" mode. This method allows tracking the increase of several key compounds PP, H_2O, HCO_2H, and CH_3OH. In this mode, specific m/z corresponding to the primary fragmentation peak of the chosen

products are selectively monitored. Specifically, we focus on m/z 18 for H_2O, m/z 29 for HCO_2H and m/z 31 for CH_3OH. For an optimized monitoring of the products, we also track the reactants CO_2 and H_2. We notice that the PP of H_2 increases significantly while the PP of other gases increases only slightly. This disparity is due to the limited compression ratio of the turbo pumps for the lightweight gases. The heavier gases tend to accumulated in the dead volume between the turbo pump exit and the isolation valve thanks to the sufficient compression. However, the turbo pump lacks the necessary compression ratio to retain H_2 in this manner which leads to an increase in the PP of H_2.

To establish a reference point, the PP of CO_2 gas is used, and the PP of the reaction products are divided by the PP of CO_2 to assess their evolution over time. Prior all these experiments, a thorough cleaning protocol was carried out on the environmental system including the E-cell where the sample was deposited. The system was first evacuated and purged with argon gas, then the sample was heated to 120°C for 30 minutes to remove water and other contaminants from the synthesis and preparation process. After the cleaning step, the gas mixture was introduced into the E-cell at a flow rate of 0.05 cm^3/min.

3. Results

3.1 Nanocatalysts initial state

STEM-HAADF imaging (Figure 1a) reveals chains of nanospheres with an average length of 700 ± 200 nm, composed of nanospheres averaging 34 ± 4 nm in diameter. These particles exhibit a discontinuous shell morphology. The shell structure (outlined by a black arrow) formed by interconnected nanoparticles (NPs) is well-defined with a measured thickness of 5 ± 2 nm, while the embedded NPs (highlighted by yellow lines in Figure 1b) exhibit an average diameter of 2 ± 1 nm. The High-resolution STEM-HAADF imaging (Figure 1b) implies the presence of porosity, marked by yellow arrows. The size distributions of NP diameters and shell thickness,presented in the insets of Figures 1b, were obtained through a statistical analysis of HAADF-STEM images. A representative set of over 100 nanospheres was analyzed to ensure statistical relevance and allow for accurate quantification of both NP diameter and nanosphere shell thickness. Electron tomography further characterizes the porosity and connectivity of nanochannels, confirming also HNS structure. A 3D reconstruction (Figure 1c) of three Pt-based HNS from an assembled chain reveals a central void, as confirmed by cross-sectional slices (Figures 1d and 1e). The measured nanosphere diameter (32 ± 2 nm) aligns with STEM-HAADF data. Radial channels (such as identified by a white arrow in Figure 1e) extend toward the inner void and frequently exceed the shell thickness (6 ± 1 nm). Statistical analysis of the reconstructed volume reveales an average of 14 channels per nanosphere. Channels diameter were measured from multiple slices extracted along different orthogonal directions within the 3D volume to minimize directional bias. This approach resulted in an average channel diameter of 8±2 nm. EDS analysis conducted on multiple, especially distinct regions of the sample, including both core and peripheral areas of several individual nanospheres, reveals an average Co content of 7 ± 3 at. %. This multi-point sampling approach helps account for local compositional variations and ensures a more representative average elemental composition across the nanosphere. This small amount of Co detected in

all HNS results from the synthesis route, which used Co NPs as sacrificial templates. The residual Co content embedded within the nanospheres indicates that there was an incomplete consumption of the Co during synthesis process [18].

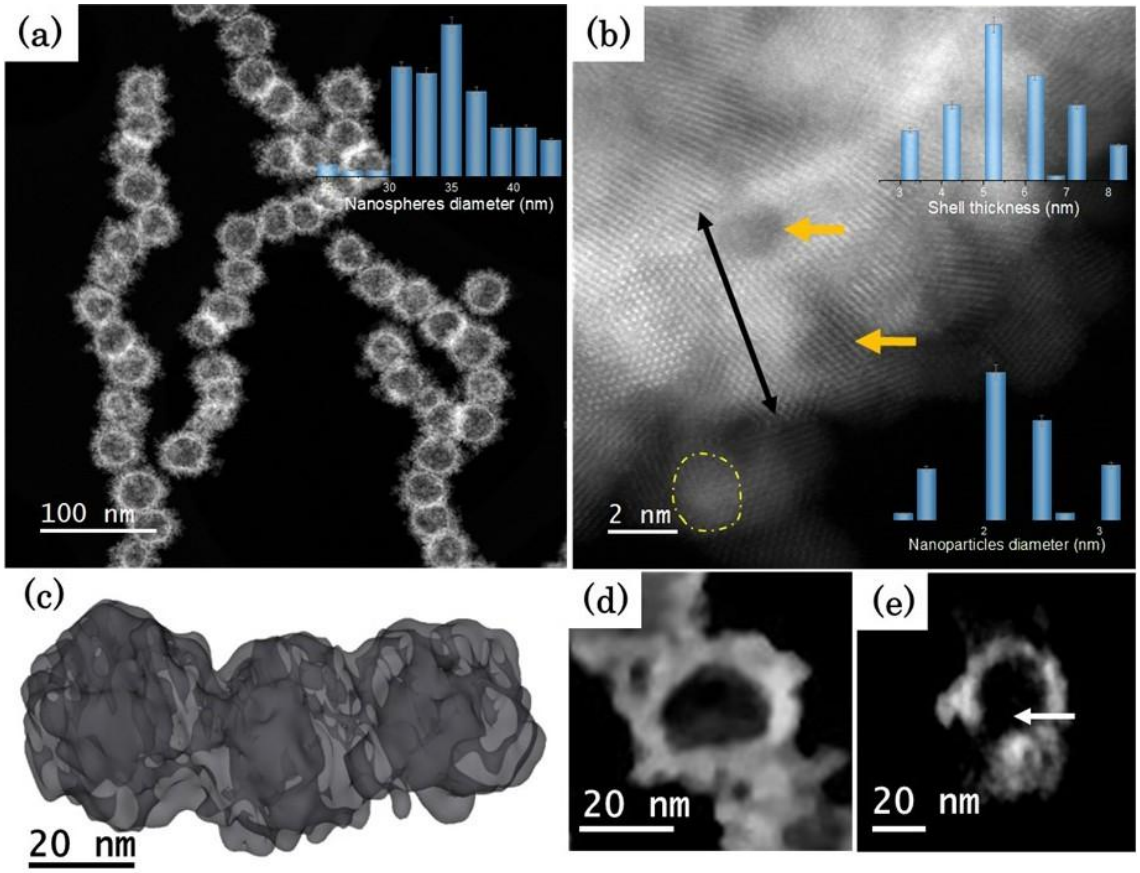

Figure 1: *Representative STEM-HAADF micrographs illustrating (a) chains of Pt-based hollow nanospheres, with an inset showing their diameter distribution, (b) high-resolution STEM images of a single hollow nanosphere shell (outlined by a black arrow) composed of interconnected NPs (outlined by yellow line) along with insets showing NP diameter and shell thickness distributions; porosity is marked by yellow arrows. (c) 3D reconstruction from ET data of three Pt based hollow nanospheres. Slices from the reconstructed volume of a nanosphere assembly in different orientations highlight (d) the central void and (e) large open channel (white arrow) providing access to the inner cavity.*

3.2 CO_2 hydrogenation reaction over Pt-based hollow nanospheres via in situ TEM

After introducing the appropriate gas composition into the environmental cell, the CO_2 hydrogenation reaction and its pathway are analysed using the residual gas analyser (RGA). This experiment is necessary before presenting the morphological evolution of the Pt-based HNS during the reaction. The resulting spectrum from an analytical scan at 300°C is presented in figure S1. This scan is performed, simultaneously with the TEM morphological analysis, to identify the reaction products. It presents the different peaks corresponding to

the reactants (CO_2 and H_2) along with their primary and secondary fragmentations. Additionally, it reveals peaks corresponding to formic acid HCO_2H (highlighted in green), water H_2O (highlighted in blue) and methanol CH_3OH (highlighted in pink). The reaction products analyses are conducted simultaneously while monitoring the morphological evolution of the Pt-based HNS.

Figure 2 presents the evolution of the anticipated CO_2 hydrogenation reaction products over time and across different temperatures. The data is normalized to the CO_2 signal. In Figure 2a, the signal corresponding to H_2O and HCO_2H is shown. It reveals a PP rise for HCO_2H starting at approximately 180°C ± 10°C (highlighted in red) which signify the onset temperature for this reaction product. The water signal, a by-product of the CO_2 hydrogenation reaction, presented a modest increase during the reaction.

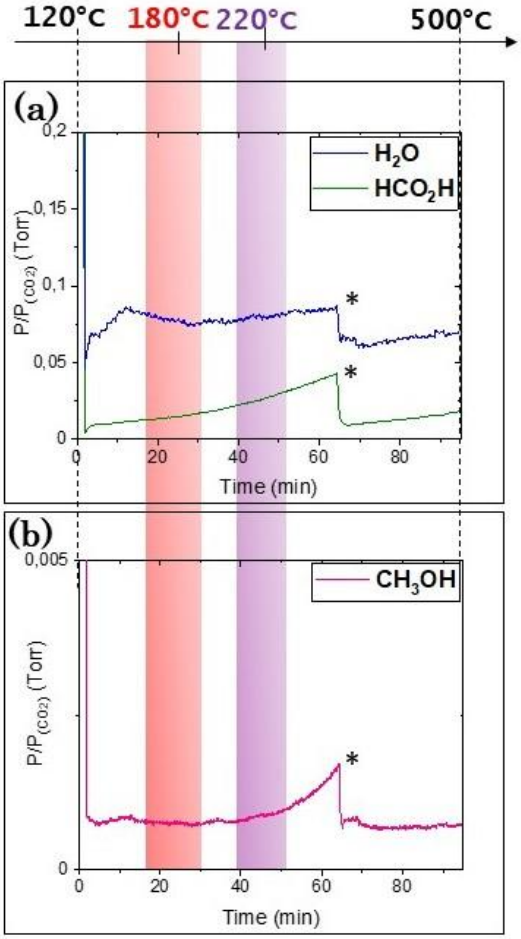

Figure 2: *RGA spectra illustrating the evolution of the Partial Pressure of (a) HCO_2H and H_2O; and (b) CH_3OH over time and temperature. The initial rise of the partial pressure of both HCO_2H and CH_3OH are highlighted by the red and purple columns, respectively, indicating the onset reaction temperature for each product. The temperatures shown on the upper part are shared across the spectra presented below. * The partial pressure drop at this point is due to the RGA safety mechanism, which limits reading upon exceeding a predefined pressure threshold*

Lastly, Figure 2b exhibits the PP of methanol, showing an increase starting at around 220°C ± 10°C (highlighted in purple), which serves as the reaction onset temperature for this particular product. The fluctuations observed in Figure 2 are attributed to another limitation of the RGA, which serves as a safety measure. When the system reaches a certain pressure level, it is pumped down to prevent the device from damage.

3.3 Pt-based hollow nanospheres morphological evolution during CO_2 hydrogenation

The evolution of the Pt-based hollow nanospheres is studied under the CO_2 hydrogenation reaction conditions during a controlled thermal treatment. STEM-HAADF images are acquired at each temperature for the observation and analysis of the morphological changes of Pt-based HNS. Although we attempted to track the system's evolution at atomic resolution during the in-situ reaction, limitations inherent to the experimental setup prevented acquisition of suitable high-resolution data. Specifically, the thickness of the environmental cell in gas-phase TEM reduced imaging resolution under reaction conditions, and the shell's complex morphology formed by multiple, misoriented nanoparticles with continuously evolving crystallographic orientations hindered consistent alignment along a zone axis. As a result, atomic-resolution imaging of the void edge and shell structure was not feasible. We therefore focused our analysis on the morphological evolution which could be reproducibly characterized throughout the reaction.

In Figure 3, only STEM-HAADF images showing remarkable morphological changes of the sample as a function of temperature are presented. Starting at 180°C, a prominent mobility of NPs is observed as indicated by the blue arrows in Figures 3a-3c. This mobility leads to the fusion of NPs with their neighboring counterparts. Additionally, two separate NPs are highlighted by white circles in their initial state in Figure 3a. These NPs exhibit a progressive reduction in size as the temperature increase, starting 180°C (Figure 3b), eventually leading to their disappearance (Figure 3c). However, precise tracking of the size reduction dynamics is challenging dur to the rapid nature of this process. Also, the limited number of observable regions where this phenomenon occurred restricts the statistical analysis. A continuous shell is formed at 340°C (indicted by a red arrow in Figure 3d), and eventually, at 500°C, we observe a partial collapse of the hollow nanosphere structure (deformed inner void outlined by green lines). Analysis of multiple regions confirms the consistent behavior of the nanoparticles at the specified temperatures. The majority of hollow nanospheres collapsed at approximately 500°C, while only around 25% exhibited partial collapse. The 2D projections of multiple nanospheres reveal the presence of open channels remaining accessible even at higher temperatures (up to 260°C).

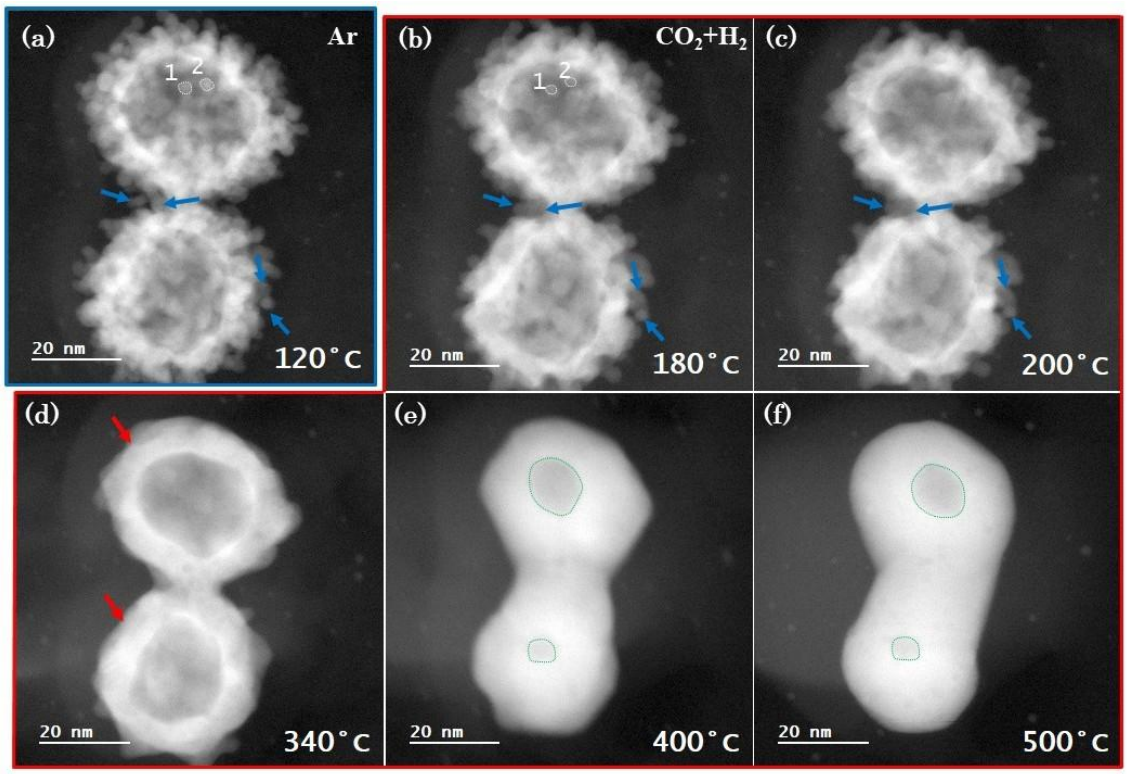

Figure 3: *Selected STEM-HAADF micrographs showing the morphological evolution of Pt-based HNS during temperature ramping from 120°C to 500°C under (CO_2 - H_2) gas mixture. The NPs 1 and 2 shrinkage and disappearance are indicated by the white circles, the mobile NPs are indicated by the blue arrows, the continuous shell is indicated by the red arrow and the partial anisotropic collapse of HNS is indicated by the green arrows*

All statistical analyses of NPs sintering and structural collapse were conducted across approximately eight distinct regions on the E-chip to ensure representative sampling and minimize localized bias. These regions were carefully selected to reflect the overall behavior of the sample while also optimizing acquisition time at each critical temperature.

In order to evaluate the potential impact of electron beam exposure on the Pt-based HNS, regions of the sample that had not been exposed to the beam were compared with irradiated areas. The analysis shows no remarkable differences in structural or morphological characteristics. This suggests that beam-induced effects are negligible under the applied experimental conditions.

3.4 Isothermal CO_2 hydrogenation

Figure 4a presents a series of representative STEM-HAADF micrographs illustrating the morphological evolution of three connected HNS during a 3-hour isothermal treatment at 180°C.

The NPs diameters, indicated by black lines in Figure 5a, were systematically measured at each time interval of 20 minutes to assess their growth behavior. Using the complete set of micrographs, the mean NP diameter was determined at successive time points. Its temporal

evolution is presented in Figure 4b. The data reveal a distinct two-stage growth pattern (marked by red lines in Figure 4b). The initial NP diameter of approximately 3.5 nm increases progressively to a final size of ~5 nm. The first stage of growth is characterized by a rapid increase in size mainly driven by the coalescence of adjacent nanoparticles. This coalescence occurs via a single-step fusion mechanism, characterized by the addition of numerous atoms to the particles in a single step. This mechanism contrasts with Ostwald ripening, where the growth or shrinkage of individual particles is characterized by a more gradual and continuous net addition or loss of atoms, resulting in a smoother growth curve. [19]; [20]; [21]

Following the rapid size increase, mild fluctuations in size are observed before a more stable and sustained particle morphology is formed and maintained throughout the remaining 2-hour thermal treatment period.

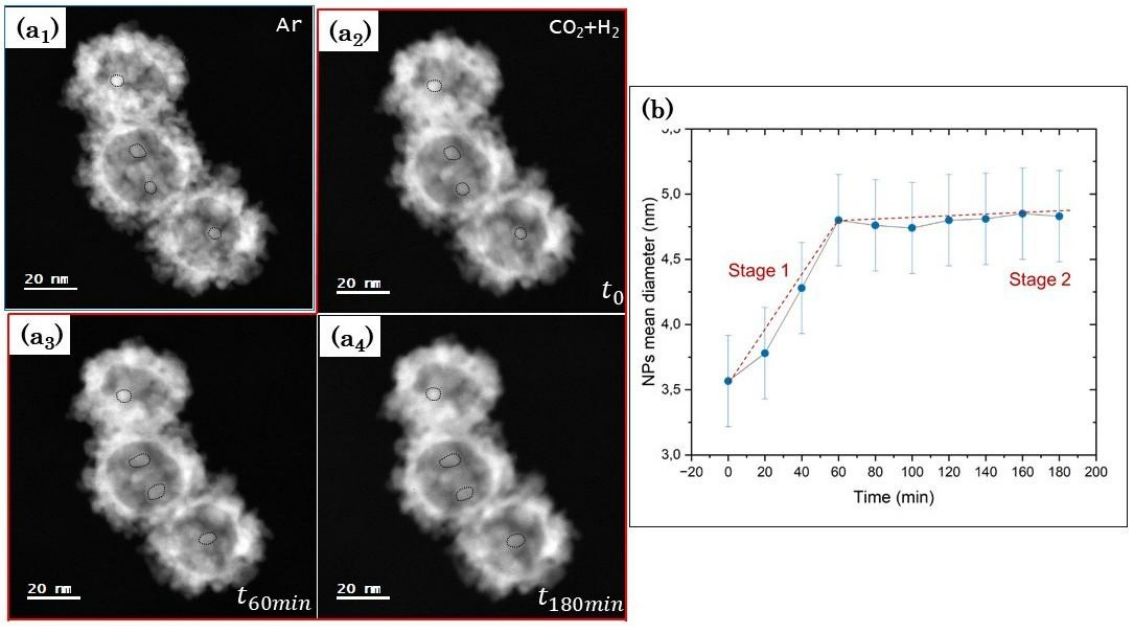

Figure 4: *(a_1-a_4) STEM-HAADF micrographs showing the morphological evolution of Pt-based HNS as a function of time at 180°C during the CO_2 hydrogenation reaction. Black lines indicate the nanoparticles. (b) Time-dependent plot of the average NP diameter forming the Pt-based HNS shell. The red lines indicate the two growth stages.*

Simultaneously, within this process, an examination of the products resulting from the CO_2 hydrogenation reaction is conducted using the RGA. The evolution of all three products (HCO_2H, CH_3OH, and H_2O) is continuous over the 3 hours of the experiment (figure 5).

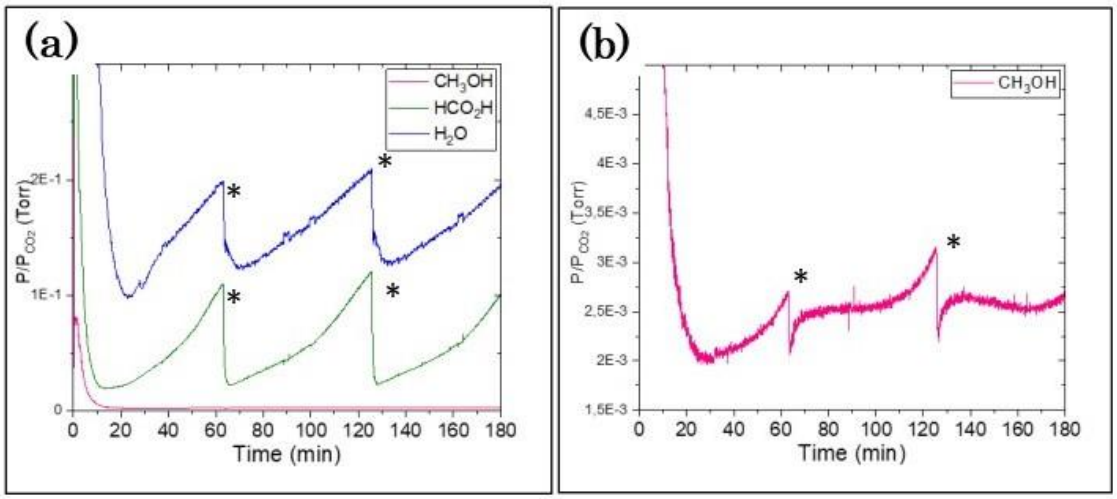

Figure 5: *(a)(b) RGA spectra illustrating the evolution of PP for CO_2 hydrogenation reaction products during 3 hours isothermal reaction at 180°C over Pt-based HNS. * The partial pressure drop at this point is due to the RGA safety mechanism, which limits reading upon exceeding a predefined pressure threshold.*

The underlying technical explanation for the fluctuations in product partial pressures has been previously discussed in this paper. The response of the reaction to the morphological changes in the catalyst is consistent, as evidenced by the continuous increase in products PP. Additionally, the ionization of CO_2 gas within the E-cell can generate CO ions, which are among the most common surface poisons for Pt-based catalysts [22]; [23]. However, the sustained increase in reaction products observed during both thermal treatment and isothermal conditions effectively eliminates catalyst deactivation caused by CO surface poisoning. It is worth noting that the thermal degradation of these nanocatalysts influences the active surface area, which typically affects the catalyst activity. However, given that the RGA is primarily utilized for qualitative analysis of the products, any smooth changes in reaction yield cannot be accurately detected.

4. Discussion

The initial state analysis of the synthesized nanocatalysts revealed the presence of multiple large channels per nanosphere, ensuring open access to the inner cavity thereby promoting efficient gas diffusion during the CO_2 hydrogenation reaction. To mimic reaction conditions within the environmental cell, a H_2/CO_2 ratio of 4 was used instead of the commonly used ratio of 3 in ex situ experiments, as increasing the H_2/CO_2 ratio enhances conversion of CO_2 to methanol at lower temperatures [24]. When considering the fact that CO_2 is chemically inert, it has been proved that increasing the reaction temperature above 200°C enhances significantly the CO_2 activation and, consequently, thereby promoting the formation of methanol [25].

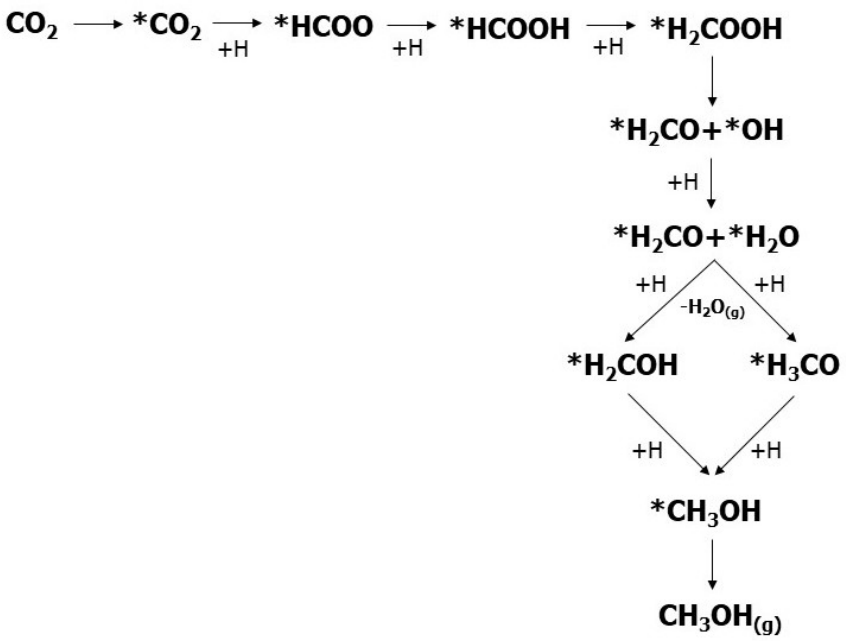

Figure 6: *Formate pathways for methanol synthesis through the CO_2 hydrogenation reaction. * indicates the adsorbed state of the molecules.*

This temperature-dependent behavior supports our findings, where methanol production was detected at 220°C, confirming it as the onset temperature for this reaction pathway under our experimental conditions. The detection of HCO_2H as reaction products certify the occurrence of the CO_2 hydrogenation reaction through the Formate pathway (Figure 6).

The formation of *HCOO from $*CO_2$ and *H over Pt-based catalysts follows a series of elementary steps. These steps involve both bond dissociation and bond formation: the breaking of C–Pt and H–Pt bonds and the formation of O–Pt and C–H bonds.

When following the Formate pathway, starting from the initial state of CO_2* and H* co-adsorption, an interaction occurs where H* is drawn towards the carbon atom of CO_2* leading to the formation of an *HCOO adduct. The co-adsorption energy (E_{ads}) for the combination of CO_2* and H* is -0.60 eV, which is lower than the adsorption energy of pure CO_2* (-0.52 eV). This suggests that the presence of the H* adatom stabilizes the adsorption of CO_2*, potentially enhancing its reactivity by spreading electrons around the adsorbed CO_2* [26]; [27].

Afterwards, *HCOO in hydrogenated, forming either $*HCO_2H$ or $*H_2COO$. It is noteworthy that the reaction *HCOO + *H → *HCOOH + * is more favorable with a lower energy change (ΔE = 0.07 eV) and a lower activation energy (E_a = 0.95 eV) than the alternative reaction *HCOO + *H → $*H_2COO$ + * (ΔE = 1.75 eV; E_a = 2.61 eV) [28].

Consequently, HCOOH* is generated when H* approaches the oxygen atom of HCOO*. Subsequently, the bond between carbon and oxygen in HCOOH* can be broken to produce HCO* and OH*, this dissociation step faces a high-energy barrier. It's worth noting that the barrier for HCOOH* dissociation is higher than its desorption. This indicates that HCOOH* is released into the gas phase before undergoing dissociation. Further hydrogenation of

HCOOH* leads to the formation of *H_2COOH intermediates, which dissociate into *H_2CO and *OH. When *H_2CO is generated, it serves as a precursor for the production of *CH_3OH through continued hydrogenation. In qualitative terms, the conversion of CO_2 to CH_3OH through the Formate pathway is limited by the hydrogenation of *HCOOH to *H_2COOH, as these processes are associated with high activation energies. [28]

This clarifies the reason behind the significant increase in HCO_2H PP signal when compared to the considerably modest signal of CH_3OH.

Several theoretical and experimental studies have provided compelling evidence that the CO_2 hydrogenation reaction over Pt-based catalysts proceeds predominantly through the Formate pathway. DFT calculations and mechanistic analysis of Pt-containing UiO-67 MOFs have shown that formate is a crucial intermediate and its hydrogenation represents the rate-determining step toward methanol formation [29]. Similarly, Pt-promoted Co–Al catalysts exhibit enhanced activity and selectivity toward methanol and higher alcohols, a performance attributed to the promotion of hydrogen spillover by Pt. This effect facilitates the generation and coupling of critical intermediates such as *HCOO, *CH_3, and *CO supporting a mechanism involving formate as a key species [30]. Furthermore, DFT studies on Pt_4 on the single vacancy graphene systems have confirmed that CO_2 hydrogenation is energetically favored via Eley-Rideal and termolecular mechanisms over the Langmuir-Hinshelwood pathway. These pathways involve intermediates such as HCOOH and HCOH with relatively low energy barriers which supports that the Formate pathway is likely to occur under practical conditions [31]. Collectively, these findings reinforce the role of formate as a central intermediate in CO_2 hydrogenation over Pt-based catalysts and align with the mechanistic trends observed in our own study.

The current study is limited to qualitative product detection due to the sensitivity constraints of the residual gas analyzer (RGA), which prevents accurate quantification of methanol yield, selectivity, and turnover frequency (TOF). To establish detailed structure–activity correlations, future investigations should incorporate more sensitive analytical tools, such as gas chromatography (GC) or GC-MS, to enable comprehensive kinetic and selectivity analyses.

While monitoring, simultaneously with the product analysis, the evolution of the Pt-based HNS, we have established that the thermal deactivation of the latter occurs due to two main factors: the reduction in catalytic surface area due to NPs growth known by NPs “sintering”, which leads to continuous shell formation and channel blockage, and the collapse of the hollow cavity. The growth of metal crystallites in this study can be attributed to two primary mechanisms: nanoparticle migration and atomic migration.

Nanoparticle migration involves the movement of entire nanoparticles across the support surface, followed by collision and fusion. It is known by particles migration and coalescence (PMC). This migration of entire particles can be attributed to thermally induced atom diffusion on the particle surfaces. The accumulation of diffusing atoms on one side of a particle causes a shift in the particle’s center, resulting in Brownian motion [32]. The mobility of NPs in this study prior their collision indicates their sintering following the PMC mechanism.

Atomic migration involves the detachment of metal atoms residing on the surface crystal planes of a particle, referred to as an 'adatoms', from the particle and moves toward another particle where it is adsorbed [33], this in known by the Ostwald ripening (OR) process. The infrequent reduction of some NPs size implicates the OR ripening mechanism governing the growth of these particles.

The presence of 20% CO_2 has slightly promoted the OR phenomenon evidenced by the shrinkage of NPs at the periphery of HNS in certain regions. When NPs coalescence occurs via surface diffusion, the activation energy (E_a) can be estimated by measuring the critical distance between coalescing NPs in STEM images at different temperatures and using these values to create an Arrhenius-type plot. In our case, we determined an activation energy of about 180 meV for the coalescence of Pt NPs under a mixed H_2 and CO_2 atmosphere (80% H_2 and 20% CO_2) (Figure SI 2). This value is intermediate when compared to those obtained under pure environments, 300 meV in vacuum and 170 meV in pure H_2 [18].

While our current work does not directly probe the impact of CO_2 adsorption on Pt surface diffusion, literature [34]; [35] suggests that CO_2 adsorption can modify the local electronic environment and availability of surface sites. Considering the reaction environment contains a mixture of approximately 20% CO_2 and 80% H_2, and given that CO_2 is generally less reactive than hydrogen, it remains plausible that CO_2 adsorption may inhibit Pt atom mobility and influence nanoparticle sintering or restructuring. However, direct experimental or theoretical evidence explicitly linking CO_2 adsorption to reduced Pt surface diffusion is currently limited. We therefore highlight the need for future studies employing surface-sensitive techniques and computational modeling to elucidate the extent and mechanism of this effect.

Following the same reasoning, the triggering temperatures for NP sintering and the structural collapse of Pt-based HNSs in a CO_2 and H_2 gas mixture were found to be consistently higher than those observed in a pure H_2 environment. Specifically, NP sintering initiated at 180 °C under the mixed gas conditions (80% H_2 / 20% CO_2), whereas in a 100% H_2 atmosphere, sintering began at a lower temperature of 160 °C. This 20 °C increase confirms the notable suppressive effect of CO_2 on NP surface diffusion and coalescence.

A similar trend was observed for the collapse of the HNS structures: in the gas mixture, collapse occurred at 500 °C, while in pure H_2 it was triggered at 400 °C, as reported in a previous study [18]. These results suggest can be attributed to CO_2's relatively low reactivity and its potential to adsorb onto Pt surfaces, thereby blocking active sites and hindering the surface diffusion of NPs. Additionally, CO_2 may alter the local chemical environment by competing with hydrogen for surface interactions, reducing the availability of adsorbed hydrogen species that would otherwise facilitate NP mobility. As a result, higher thermal energy is required to overcome the diffusion barrier, explaining the elevated activation energy and delayed onset of structural changes observed under mixed gas conditions.

Residual Co, present at approximately 7±3 at. %, may influence Pt catalytic activity through alloying and electronic effects. Previous studies [36]; [37]; [38]; [39] have demonstrated that under reducing atmospheres, Pt and Co can form intermetallic alloys as Co oxides are reduced and incorporated into the metallic phase, while Pt tends to segregate on nanoparticle surfaces at lower temperatures. In our system, the annealing temperature of 300 °C is likely

insufficient to fully reduce and homogenize Co oxides, especially in the presence of CO_2 which inhibits complete reduction. However, treatment at 500 °C facilitates the reduction of Co oxides and their redistribution via hydrogen-induced diffusion, favoring alloy formation. This suggests that residual Co primarily participates in alloying rather than remaining as inert or interfering residues.

The Pt-based HNS presented nanospheres categorized as 'half stable' in accordance with the classification proposed by Jiang et al [40]. This classification is due to the anisotropic nature of the HNS collapse. Other 'unstable' HNS structures with thinner shells underwent a more rapid isotropic collapse, resulting in the formation of solid nanoparticles at the same temperature [18].

Reports comparing hollow nanospheres to their solid counterparts have demonstrated that hollow structures generally possess higher surface areas and exhibit superior catalytic performance largely attributed to this increased surface accessibility [41]; [42]; [43]; [44]; [45]; [46]. In our system, the collapse of hollow nanospheres into solid nanoparticles likely results in a significant reduction in accessible surface area, which may contribute to decreased catalytic activity and alterations in the long-range crystallinity of the material.

Although nanoparticle sintering and structural collapse have been identified as the primary deactivation mechanisms, the potential influence of CO adsorption on the Pt surface cannot be fully excluded. While residual gas analysis did not detect any significant CO accumulation in the gas phase, it is possible that CO may exist in an adsorbed state under reaction conditions. However, previous studies on Pt-based catalysts [47]; [48] have demonstrated that CO adsorption is generally weak at elevated temperatures and in hydrogen-rich environments and CO is more likely to undergo further reaction rather than accumulate on the surface. Nevertheless, further investigations using surface-sensitive techniques such as DRIFTS or XPS would be valuable to conclusively determine the presence and role of surface-adsorbed CO in the deactivation process.

5. Conclusions

This study provides a comprehensive analysis of the thermal stability and catalytic behavior of Pt-based HNS under CO_2 hydrogenation conditions. The in situ and operando TEM approach has enabled real-time observation of NPs migration, sintering, and eventual collapse of the hollow structure, leading to catalytic deactivation. Indications of NPs shrinkage prior to their disappearance imply the growth of NPs following the OR mechanism. Reaction analysis confirms that CO_2 hydrogenation proceeds via the Formate pathway with formic acid as a key intermediate. The onset of significant morphological changes at 180°C coincides with the beginning of CO_2 hydrogenation activity. This highlights the temperature-dependent evolution of the catalyst during the early stages of the reaction. Furthermore, the temperatures at which NP sintering and HNS collapse were triggered were significantly higher in the CO_2-H_2 gas mixture. In the latter, sintering started occurring at 180°C and collapse at 500°C compared to 160°C and 400°C in pure H_2, respectively [18]. The primary deactivation mechanisms identified include the coalescence of Pt NPs, loss of accessible active sites and structural collapse of the HNS framework. Furthermore, the CO_2 ionization

within the E-cell can generate CO ions which is a known surface poison for Pt-based catalysts. The sustained production of reaction products throughout the process suggests that CO poisoning does not significantly contribute to catalyst deactivation under the studied conditions. These findings emphasize the necessity for enhanced catalyst design strategies such as stabilizing nanoparticle dispersion and optimizing structural robustness to improve catalytic longevity. The insights gained in this study contribute to the ongoing development of efficient and durable catalysts for sustainable methanol synthesis from CO_2.

Acknowledgements

Bernhard Witulski (LCMT, Caen) is gratefully acknowledged for his valuable contributions to the synthesis of Pt-based hollow nanospheres and for the insightful discussions. This research was partially supported by the CNRS federation IRMA — FR 3095, and supported by Conseil Régional de Normandie (France), European FEDER funding, and the French Agence Nationale de la Recherche Labex EMC3 through project ZEOMAH (ANR-10-LABX-09-01). GENESIS is supported by the Région Haute-Normandie, the Métropole Rouen Normandie, and the French National Research Agency as a part of the program "Investissements d'avenir" (ANR-11- EQPX-0020).

Supplementary materials

Figure S1. Analog spectrum of the gas at the cell's outlet, highlighting the peaks that correspond to CO_2 hydrogenation reaction products over Pt nanospheres registered at 300°C (green for HCO_2H, blue for H_2O and pink for CH_3OH). Figure S2. (a) STEM micrographs utilized to measure interparticle distances (x). (b) Linearized Arrhenius Plot, with the Estimated Activation Energy from ln(x) vs 1/T.

Data availability

Data will be made available on request.

References

[1] P. Frontera, A. Macario, M. Ferraro, P.L. Antonucci, Supported Catalysts for CO2 Methanation: A Review, Catalysts. 7 (2017). https://doi.org/10.3390/catal7020059.

[2] M. González-Castaño, B. Dorneanu, H. Arellano-García, the reverse water gas shift reaction: a process system engineering perspective, Reaction Chemistry Engineering. 6 (2021) 954–976. https://doi.org/10.1039/d0re00478b.

[3] M. Bowker, Methanol Synthesis from CO2 Hydrogenation, ChemCatChem. 11 (2019). https://doi.org/10.1002/cctc.201900401.

[4] D. Xu, Y. Wang, M. Ding, X. Hong, G. Liu, S.C.E. Tsang, Advances in higher alcohol synthesis from CO2 hydrogenation, Chem. 7 (2021). https://doi.org/10.1016/j.chempr.2020.10.019.

[5] R. Sun, Y. Liao, S.-T. Bai, M. Zheng, C. Zhou, T. Zhang, B.F. Sels, Heterogeneous catalysts for CO2hydrogenation to formic acid/formate: from nanoscale to single atom, Energy Environmental Science. 14 (2021) 1247–1285. https://doi.org/10.1039/d0ee03575k.

[6] H. Yang, C. Zhang, P. Gao, H. Wang, X. Li, L. Zhong, W. Wei, Y. Sun, A review of the catalytic hydrogenation of carbon dioxide into value-added hydrocarbons, Catalysis Science Technology. 7 (2017) 4580–4598. https://doi.org/10.1039/c7cy01403a.

[7] L.H. Vieira, L.F. Rasteiro, C.S. Santana, G.L. Catuzo, A.H.M. da Silva, J.M. Assaf, E.M. Assaf, Noble Metals in Recent Developments of Heterogeneous Catalysts for CO2Conversion Processes, ChemCatChem. 15 (2023). https://doi.org/10.1002/cctc.202300493.

[8] S. Kattel, B. Yan, Y. Yang, J.G. Chen, P. Liu, Optimizing Binding Energies of Key Intermediates for CO2 Hydrogenation to Methanol over Oxide-Supported Copper, Journal of the American Chemical Society. 138 (2016). https://doi.org/10.1021/jacs.6b05791.

[9] L.F. Rasteiro, M.A.L.S. Rossi, J.M. Assaf, E.M. Assaf, Low-pressure hydrogenation of CO2 to methanol over Ni-Ga alloys synthesized by a surfactant-assisted co-precipitation method and a proposed mechanism by DRIFTS analysis, Catalysis Today. 381 (2021). https://doi.org/10.1016/j.cattod.2020.05.067.

[10] A. Álvarez, A. Bansode, A. Urakawa, A.V. Bavykina, T.A. Wezendonk, M. Makkee, J. Gascon, F. Kapteijn, Challenges in the Greener Production of Formates/Formic Acid, Methanol, and DME by Heterogeneously Catalyzed CO2Hydrogenation Processes, Chemical Reviews. 117 (2017). https://doi.org/10.1021/acs.chemrev.6b00816.

[11] T. Toyao, S. Kayamori, Z. Maeno, S.M.A.H. Siddiki, K.-ichi Shimizu, Heterogeneous Pt and MoOx Co-Loaded TiO2 Catalysts for Low-Temperature CO2 Hydrogenation To Form CH3OH, ACS Catalysis. 9 (2019). https://doi.org/10.1021/acscatal.9b01225.

[12] Y.-L. Men, Y. Liu, Q. Wang, Z.-H. Luo, S. Shao, Y.-B. Li, Y.-X. Pan, Highly dispersed Pt-based catalysts for selective CO2 hydrogenation to methanol at atmospheric pressure, Chemical Engineering Science. 200 (2019). https://doi.org/10.1016/j.ces.2019.02.004.

[13] E.S. Gutterød, A. Lazzarini, T. Fjermestad, G. Kaur, M. Manzoli, S. Bordiga, S. Svelle, K.P. Lillerud, E. Skúlason, S. Øien-Ødegaard, A. Nova, U. Olsbye, Hydrogenation of CO2 to Methanol by Pt Nanoparticles Encapsulated in UiO-67: Deciphering the Role of the Metal–Organic Framework, Journal of the American Chemical Society. 142 (2019). https://doi.org/10.1021/jacs.9b10873.

[14] J.R. Crockett, M. Wang, J.E. Doebler, T. Pawale, X. Li, Y. Bao, Impact on the Formation and Catalytic Property of Pt-Based Nanocatalysts by Galvanic Reaction with Co-Reduction Agents, Chemistry of Materials. 34 (2022). https://doi.org/10.1021/acs.chemmater.2c02659.

[15] M. Xiao, Z. Wang, M. Lyu, B. Luo, S. Wang, G. Liu, H.M. Cheng, L. Wang, Hollow Nanostructures for Photocatalysis: Advantages and Challenges, Advanced Materials. 31 (2018). https://doi.org/10.1002/adma.201801369.

[16] S. Cohen-Pope, J.R. Crockett, M. Wang, K. Flynn, A. Hoff, Y. Bao, Morphology control of SERS-active 2D gold nanosnowflakes, Journal of Materials Chemistry C. 8 (2020) 12427–12436. https://doi.org/10.1039/d0tc02183k.

[17] S. Tominaka, Y. Nakamura, T. Osaka, Nanostructured catalyst with hierarchical porosity and large surface area for on-chip fuel cells, Journal of Power Sources. 195 (2010). https://doi.org/10.1016/j.jpowsour.2009.08.082.

[18] J. Rezkallah, X. Sauvage, B. Witulski, S. Moldovan, Insights on Morphology and Thermal Stability of Hollow Pt Nanospheres by In Situ Environmental TEM, Molecules. 30 (2025). https://doi.org/10.3390/molecules30040792.

[19] S.B. Simonsen, I. Chorkendorff, S. Dahl, M. Skoglundh, J. Sehested, S. Helveg, Ostwald ripening in a Pt/SiO2 model catalyst studied by in situ TEM, Journal of Catalysis. 281 (2011). https://doi.org/10.1016/j.jcat.2011.04.011.

[20] P. Wynblatt, N.A. Gjostein, Particle growth in model supported metal catalysts—I. Theory, Acta Metallurgica. 24 (1976). https://doi.org/10.1016/0001-6160(76)90034-1.

[21] S.B. Simonsen, Y. Wang, J.O. Jensen, W. Zhang, Coarsening of carbon black supported Pt nanoparticles in hydrogen, Nanotechnology. 28 (2017). https://doi.org/10.1088/1361-6528/aa91a8.

[22] S. Xu, S. Chansai, S. Xu, C.E. Stere, Y. Jiao, S. Yang, C. Hardacre, X. Fan, CO Poisoning of Ru Catalysts in CO2 Hydrogenation under Thermal and Plasma Conditions: A Combined Kinetic and Diffuse Reflectance Infrared Fourier Transform Spectroscopy–Mass Spectrometry Study, ACS Catalysis. 10 (2020). https://doi.org/10.1021/acscatal.0c03620.

[23] S.W. Chee, J.M. Arce-Ramos, W. Li, A. Genest, U. Mirsaidov, Structural changes in noble metal nanoparticles during CO oxidation and their impact on catalyst activity, Nature Communications. 11 (2020). https://doi.org/10.1038/s41467-020-16027-9.

[24] M. Tommasi, S.N. Degerli, G. Ramis, I. Rossetti, Advancements in CO2 methanation: A comprehensive review of catalysis, reactor design and process optimization, Chemical Engineering Research and Design. 201 (2024). https://doi.org/10.1016/j.cherd.2023.11.060.

[25] J. Ma, N. Sun, X. Zhang, N. Zhao, F. Xiao, W. Wei, Y. Sun, A short review of catalysis for CO2 conversion, Catalysis Today. 148 (2009). https://doi.org/10.1016/j.cattod.2009.08.015.

[26] J. Ye, C.-jun Liu, D. Mei, Q. Ge, Methanol synthesis from CO2 hydrogenation over a Pd4/In2O3 model catalyst: A combined DFT and kinetic study, Journal of Catalysis. 317 (2014). https://doi.org/10.1016/j.jcat.2014.06.002.

[27] A.L. Maulana, R.I.D. Putra, A.G. Saputro, M.K. Agusta, N. Nugraha, H.K. Dipojono, DFT and microkinetic investigation of methanol synthesis via CO2 hydrogenation on Ni(111)-based surfaces, Physical Chemistry Chemical Physics. 21 (2019) 20276–20286. https://doi.org/10.1039/c9cp02970b.

[28] X. Wang, J. Pan, H. Wei, W. Li, J. Zhao, Z. Hu, Mechanism of Methanol Synthesis from CO2 Hydrogenation over Pt8/In2O3 Catalysts: A Combined Study on Density Functional Theory and Microkinetic Modeling, The Journal of Physical Chemistry C. 126 (2022). https://doi.org/10.1021/acs.jpcc.1c08098.

[29] S.H. Pulumati, D.K. Sannes, C.R. Jabbour, L.D.B. Mandemaker, B.M. Weckhuysen, U. Olsbye, A. Nova, E. Skúlason, Mechanistic Insights in the Catalytic Hydrogenation of CO2 over Pt Nanoparticles in UiO-67 Metal–Organic Frameworks, ACS Catalysis. 14 (2023). https://doi.org/10.1021/acscatal.3c03401.

[30] Y. He, B. Xu, S. Liu, W. Fu, J. Chen, J. Ren, R. Sun, Z. Tang, C. Mebrahtu, H. Chen, F. Zeng, Effects of hydrogen spillover on CO2 hydrogenation over Pt-Co-Al based catalysts, Applied Catalysis A: General. 691 (2025). https://doi.org/10.1016/j.apcata.2024.120051.

[31] G. Yan, Z. Gao, M. Zhao, W. Yang, X. Ding, CO2 hydrogenation to formic acid over platinum cluster doped defective graphene: A DFT study, Applied Surface Science. 517 (2020). https://doi.org/10.1016/j.apsusc.2020.146200.

[32] C.H. Bartholomew, Sintering kinetics of supported metals: new perspectives from a unifying GPLE treatment, Applied Catalysis A: General. 107 (1993). https://doi.org/10.1016/0926-860x(93)85114-5.

[33] A. Kabalnov, Ostwald Ripening and Related Phenomena, Journal of Dispersion Science and Technology. 22 (2001). https://doi.org/10.1081/dis-100102675.

[34] X. Liu, L. Sun, W.-Q. Deng, Theoretical Investigation of CO2 Adsorption and Dissociation on Low Index Surfaces of Transition Metals, The Journal of Physical Chemistry C. 122 (2018). https://doi.org/10.1021/acs.jpcc.7b12660.

[35] I. Kherbach, V. Climent, J.M. Feliu, CO2 reduction on adatom decorated platinum stepped surfaces, The Journal of Chemical Physics. 158 (2023). https://doi.org/10.1063/5.0147195.

[36] S. Alayoglu, S.K. Beaumont, F. Zheng, V.V. Pushkarev, H. Zheng, V. Iablokov, Z. Liu, J. Guo, N. Kruse, G.A. Somorjai, CO2 Hydrogenation Studies on Co and CoPt Bimetallic Nanoparticles Under Reaction Conditions Using TEM, XPS and NEXAFS, Topics in Catalysis. 54 (2011). https://doi.org/10.1007/s11244-011-9695-9.

[37] P. Karipoth, R.J. Joseyphus, Evolution of High Coercivity in CoPt Nanoparticles Through Nitrogen Assisted Annealing, Journal of Superconductivity and Novel Magnetism. 27 (2014). https://doi.org/10.1007/s10948-014-2564-6.

[38] X. Sun, Z.Y. Jia, Y.H. Huang, J.W. Harrell, D.E. Nikles, K. Sun, L.M. Wang, Synthesis and magnetic properties of CoPt nanoparticles, Journal of Applied Physics. 95 (2004). https://doi.org/10.1063/1.1667441.

[39] J.D. Lee, D. Jishkariani, Y. Zhao, S. Najmr, D. Rosen, J.M. Kikkawa, E.A. Stach, C.B. Murray, Tuning the Electrocatalytic Oxygen Reduction Reaction Activity of Pt–Co Nanocrystals by Cobalt Concentration with Atomic-Scale Understanding, ACS Applied Materials Interfaces. 11 (2019). https://doi.org/10.1021/acsami.9b06346.

[40] L. Jiang, X. Yin, J. Zhao, H. Liu, Y. Liu, F. Wang, J. Zhu, F. Boey, H. Zhang, Theoretical Investigation on the Thermal Stability of Hollow Gold Nanoparticles, The Journal of Physical Chemistry C. 113 (2009). https://doi.org/10.1021/jp905280g.

[41] H.P. Liang, H.M. Zhang, J.S. Hu, Y.G. Guo, L.J. Wan, C.L. Bai, Pt Hollow Nanospheres: Facile Synthesis and Enhanced Electrocatalysts, Angewandte Chemie International Edition. 43 (2004). https://doi.org/10.1002/anie.200352956.

[42] J. Zeng, Q. Zhang, J. Chen, Y. Xia, A Comparison Study of the Catalytic Properties of Au-Based Nanocages, Nanoboxes, and Nanoparticles, Nano Letters. 10 (2009). https://doi.org/10.1021/nl903062e.

[43] T.S. Rodrigues, A.G.M. da Silva, P.H.C. Camargo, Nanocatalysis by noble metal nanoparticles: controlled synthesis for the optimization and understanding of activities, Journal of Materials Chemistry A. 7 (2019) 5857–5874. https://doi.org/10.1039/c9ta00074g.

[44] K. An, T. Hyeon, Synthesis and biomedical applications of hollow nanostructures, Nano Today. 4 (2009). https://doi.org/10.1016/j.nantod.2009.06.013.

[45] Y. Sun, B. Mayers, Y. Xia, Metal Nanostructures with Hollow Interiors, Advanced Materials. 15 (2003). https://doi.org/10.1002/adma.200301639.

[46] X. Xia, Y. Wang, A. Ruditskiy, Y. Xia, 25th Anniversary Article: Galvanic Replacement: A Simple and Versatile Route to Hollow Nanostructures with Tunable and Well-Controlled Properties, Advanced Materials. 25 (2013). https://doi.org/10.1002/adma.201302820.

[47] C. Lentz, S.P. Jand, J. Melke, C. Roth, P. Kaghazchi, DRIFTS study of CO adsorption on Pt nanoparticles supported by DFT calculations, Journal of Molecular Catalysis A: Chemical. 426 (2017). https://doi.org/10.1016/j.molcata.2016.10.002.

[48] I. Tankov, W.H. Cassinelli, J.M.C. Bueno, K. Arishtirova, S. Damyanova, DRIFTS study of CO adsorption on praseodymium modified Pt/Al2O3, Applied Surface Science. 259 (2012). https://doi.org/10.1016/j.apsusc.2012.07.138.